



Research paper

Silencing of circular RNA HIPK2 in neural stem cells enhances functional recovery following ischaemic stroke



Guangtian Wang^a, Bing Han^a, Ling Shen^a, Shusheng Wu^a, Li Yang^a, Jiefeng Liao^a, Fangfang Wu^a, Mingyue Li^a, Shuo Leng^b, Fengchao Zang^b, Yuan Zhang^a, Ying Bai^a, Yu Mao^c, Bo Chen^d, Honghong Yao^{a,e,f,*}

^a Department of Pharmacology, School of Medicine, Southeast University, Nanjing 210009, China

^b Department of Radiology, School of Medicine, Southeast University, Nanjing 210009, China

^c State Key Laboratory of Bioelectronics, Jiangsu Key Laboratory for Biomaterials and Devices, School of Biological Sciences & Medical Engineering, Southeast University, Nanjing 210009, China

^d Materials Science and Devices Institute, Suzhou University of Science and Technology, Suzhou 215009, China

^e Institute of Life Sciences, Key Laboratory of Developmental Genes and Human Disease, Southeast University, Nanjing 210009, China

^f Co-innovation Centre of Neuroregeneration, Nantong University, Nantong 226001, China

ARTICLE INFO

Article History:

Received 26 September 2019

Revised 15 January 2020

Accepted 22 January 2020

Available online xxx

Keywords:

Neural stem cells

Differentiation

circHIPK2

Stroke

Functional recovery

ABSTRACT

Background: Circular RNAs (circRNAs) have been reported to be involved in central nervous system (CNS) diseases and to have a close connection with neuronal development. However, the role of circRNAs in neural stem cell (NSC) differentiation and the treatment of ischaemic stroke remains unknown.

Methods: Ischaemic stroke was induced in mice using transient middle cerebral artery occlusion (tMCAO). NSCs were transduced with circHIPK2 siRNA (si-circHIPK2-NSCs) or vehicle control (si-circCon-NSCs) and microinjected into lateral ventricle of brain at 7 d post-tMCAO. Magnetic resonance imaging (MRI) was used to detect brain damage, and functional deficits were evaluated with sensorimotor behavioural tests. The distribution of the transplanted NSCs was investigated by near-infrared fluorescence imaging (NIF) and immunofluorescence. The neural plasticity of si-circHIPK2-NSCs was verified by western blot and immunofluorescence *in vivo* and *in vitro*.

Findings: We investigated the role of circHIPK2 in NSC differentiation. *In vitro*, silencing of circHIPK2 facilitated NSCs directionally differentiated to neurons but had no effect on the differentiation to astrocytes. *In vivo*, microinjected NSCs could migrate to the ischaemic hemisphere after stroke induction. Si-circHIPK2-NSCs increased neuronal plasticity in the ischaemic brain, conferred long-lasting neuroprotection, and significantly reduced functional deficits.

Interpretations: Si-circHIPK2 regulates NSC differentiation, and microinjection of si-circHIPK2-NSCs exhibits a promising therapeutic strategy to neuroprotection and functional recovery after stroke.

Funding: The National Key Research and Development Program of China; the International Cooperation and Exchange of the National Natural Science Foundation of China; the National Natural Science Foundation of China; the Jiangsu Innovation & Entrepreneurship Team Program.

© 2020 The Author(s). Published by Elsevier B.V. This is an open access article under the CC BY-NC-ND license. (<http://creativecommons.org/licenses/by-nc-nd/4.0/>)

Abbreviations: bFGF, basic fibroblast growth factor; BrdU, bromodeoxyuridine; circHIPK2, circRNA HIPK2; circRNAs, circular RNAs; CNS, central nervous system; ECA, external carotid artery; EGF, epidermal growth factor; FPKM, fragments per kilobase per million reads; GFAP, glial fibrillary acidic protein; mNSS, modified neurological severity scores; MRI, magnetic resonance imaging; NIF, near-infrared fluorescence imaging; NSCs, neural stem cells; OGD/R, oxygen and glucose deprivation-reperfusion; qPCR, quantitative polymerase chain reaction; Smox, spermine oxidase; tMCAO, transient middle cerebral artery occlusion

* Corresponding author at: Department of Pharmacology, School of Medicine, Southeast University, Nanjing 210009, China.

E-mail address: yaohh@seu.edu.cn (H. Yao).

1. Introduction

Stroke is a major cause of disability and affects nearly 795,000 people every year, leading to immense health and economic burdens in adults worldwide [1]. Intravenous administration of recombinant human tissue-type plasminogen activator within three hours of symptom onset remains the only Food and Drug Administration-approved pharmacotherapy for the clinical management of stroke. Because of its narrow therapeutic window, only approximately 7% of patients are eligible for this treatment, and the efficacy of ischaemic stroke thrombolytic therapy is limited [2]. Although many drugs

Research in context

Evidence before this study

Stroke is a destructive neurological deficit that has become a major cause of death and adult disability worldwide. However, due to the narrow treatment window and the rigorous treatment criteria, only a small percentage of stroke patients can benefit from the current treatment. Neural stem cells (NSCs) have been widely investigated for protective and regenerative strategies after stroke and have shown great promise. Circular RNAs (circRNAs) have been reported to be involved in regulating the physiological and pathophysiological processes associated with ischaemic stroke. However, the role of circRNAs in NSC differentiation and the treatment of ischaemic stroke remains unknown.

Added value of this study

The major achievements of this study are summarized below:

1. We demonstrated that circHIPK2 is involved in the differentiation of NSCs. Silencing of circHIPK2 in NSCs facilitated neuronal differentiation, and overexpression of circHIPK2 in NSCs reduced neuronal differentiation.
2. Si-circHIPK2-NSCs conferred long-lasting neuroprotection and significantly reduced functional deficits after tMCAO, revealing the potential of si-circHIPK2-NSCs as a promising treatment for ischaemic stroke.
3. We explored the mechanism underlying si-circHIPK2-NSC-induced neuroprotection, regeneration and functional recovery after ischaemic stroke and found that Smox acts as an important downstream mediator of circHIPK2.

Implications of all the available evidence

We report that late postischaemic treatment of mice with si-circHIPK2-NSCs improves functional recovery. Thus, si-circHIPK2-NSCs might offer a new approach to the treatment of stroke. This study may provide insight into the differentiation of NSCs and provide a new therapeutic method.

show significant neuroprotection in animal models, these results have not been replicated in human clinical trials [3]. Given the complex nature of postischaemic brain injury and its systemic consequences, cell-based approaches achieve greater efficacy than single pharmacological therapies by targeting multiple mechanisms [4,5].

Emerging research interests have been focused on protective and regenerative strategies using NSCs after stroke [6–8]. In human patients and animal stroke models, neurons that are supplied with blood solely by the affected artery die rapidly, whereas neurons peripheral to the core, which are also perfused to some extent by other arteries, undergo delayed apoptosis [9,10]. After stroke, endogenous quiescent NSCs become active and participate in the process of brain repair. However, the self-repair process is usually inadequate and transient [11]. NSCs may provide a cellular reservoir for the replacement of lost or damaged cells and transplanted NSCs can differentiate into neurons, astrocytes, oligodendrocytes and vascular cells by secreting trophic factors [12,13], which can reduce cell death and increase endogenous neurogenesis and angiogenesis, NSCs show great promise for the treatment of neurological disorders [3,5].

Circular RNAs (circRNAs) are a novel class of noncoding RNAs characterized by covalently closed loop structures with neither 5' to 3' polarity nor a polyadenylated tail [14,15]. Recently, studies have shown that the expression of circRNAs is widespread [16,17]. Moreover, the expression of circRNAs has recently been shown to be

tissue-specific and regulated by different biological processes, such as stroke, neuroinflammation and senescence, hypertrophy and heart failure as well as cell growth [18–23]. Although transcription factors, microRNAs, lncRNAs, and signalling pathways that control the transition between NSCs and neurogenic progenitors have been studied intensively [24–27], the role of circRNAs in NSC differentiation is still unknown.

In the present study, we investigated the role of circHIPK2 siRNA in the differentiation of NSCs and the potential of NSCs transduced with circHIPK2 siRNA (si-circHIPK2-NSCs) to promote functional recovery and neural plasticity after stroke. Moreover, we wanted to demonstrate the feasibility of tracking transplanted si-circHIPK2-NSCs *in vivo* in tMCAO-injured mice, aiming to explore its potential for clinical translation.

2. Materials and methods

2.1. Study approval

All animal procedures were performed in strict accordance with the Animal Research: Reporting of *in vivo* Experiments guidelines. The care and use of animals were reviewed and approved by the Institutional Animal Care and Use Committee at the Medical School of Southeast University (approval ID: SYXK-2010.4987).

2.2. Animals

Adult male C57BL/6 J mice (22.0 to 28.0 g, 8 to 9 weeks old) and EGFP transgenic mice were purchased from the Model Animal Research centre of Nanjing University (Nanjing, China). Adult male C57BL/6 J mice were randomly assigned to experimental groups. All animals were housed under a constant temperature and humidity and a 12 h light/12 h dark cycle, with the lights on at 7:00 AM. Food and water were available *ad libitum*.

2.3. Cell culture and NSC differentiation

Embryonic NSCs from C57BL/6 J mice and EGFP transgenic mice were isolated from the embryonic day 14 (E14) mouse hippocampus and the neonatal EGFP transgenic mouse hippocampus. Cells in suspension were cultured in proliferation medium containing 20 ng/mL basic fibroblast growth factor (bFGF; Stem cell, Canada), 20 ng/mL epidermal growth factor (EGF; Stem cell, Canada) and 2% B27 supplement (Gibco, USA) and passaged every 4–6 d these embryonic NSCs still possessed proliferative capacity. Embryonic NSCs and GFP⁺ NSCs from the 3rd to 8th passages were used in this study. For NSC differentiation, NSCs were allowed to differentiate in growth factor-free DMEM/F12 (1:1) medium containing 2% B27 (Gibco, USA) and 0.5% foetal bovine serum (HyClone, USA).

2.4. Quantitative polymerase chain reaction (qPCR)

Total RNA from cells or tissues was extracted using a previously described method [20]. RNAs were detected using qPCR. The primers used in these assays are provided in Supplementary Table 1.

2.5. Bromodeoxyuridine (BrdU) labeling

NSCs were prepared on poly-L-lysine-coated glass cover slips. A detailed method was performed using a previously described method [28].

2.6. Lentiviral transduction

NSCs were transduced with circ control siRNA and circHIPK2 siRNA lentivirus (HANBIO Inc., China) with multiplicity of infection of

0.5, followed by gentle swirling, incubation and replacement of fresh feed medium.

2.7. Western blot analysis

Samples were processed to determine cellular protein concentrations as previously described [20]. Next, equal amounts of protein were separated by SDS-PAGE under reducing conditions, and the separated proteins were transferred onto a PVDF membrane. The PVDF membranes were then blocked with 5% nonfat dry milk in Tris-buffered saline with 0.2% Tween-20 at room temperature for 1 h. The membranes were probed with antibodies specific for glial fibrillary acidic protein (GFAP), (Cat# 16825-1-AP, RRID:AB_2109646, 1:1000, Proteintech), Nestin (Cat# 66259-1-Ig, RRID:AB_2756523, 1:1000, Proteintech), TUJ1 (Cat# ab18207, RRID:AB_444319, 1:1000, Abcam), NeuN (Cat# ab104224, RRID:AB_10711040, 1:1000, Abcam), PSD-95 (Cat# ab2723, RRID:AB_303248, 1:1000, Abcam), synaptophysin (Cat# ab32127, RRID:AB_2286949, 1:1000, Abcam), Smox (Cat# 15052-1-AP, RRID:AB_2239689, 1:500, Proteintech), and β -actin (Cat# 60008-1-Ig, RRID:AB_2289225, 1:1000, Proteintech) overnight at 4°C. After four additional washes, the membranes were then incubated with horseradish peroxidase-conjugated goat anti-mouse IgG secondary antibody (Cat# SA00001-1, RRID:AB_2722565, 1:2000, Proteintech) or rabbit IgG secondary antibody (Cat# SA00001-2, RRID:AB_2722564, 1:2000, Proteintech). A chemiluminescence detection system (DNR, Israel) was used to detect the resultant signals. The individual protein bands were quantified by using ImageJ software. Each western blot was repeated at least three times.

2.8. tMCAO

tMCAO was processed according to a previous study [18]. Briefly, mice were anaesthetized with isoflurane (2–2.5%) in a mixture of O₂/N₂O (30%/70%). During the surgery and recovery period, the rectal temperature of the mice was maintained at 37 °C, and the temperature of the mouse cages was maintained with a heating blanket. A silicone-coated nylon filament was introduced into the right external carotid artery (ECA), advanced through the internal carotid artery and gently pushed up to the tMCAO. One hour after occlusion, the mice were anaesthetized again and the nylon filament was removed to achieve reperfusion. In sham-operated mice, the ECA was twisted with an electrocoagulation pen, but a nylon filament was not inserted into the ECA. All groups were monitored for physiological parameters before tMCAO and for 1 h after reperfusion. Sham-operated mice served as controls.

2.9. Microinjection of NSCs

Si-circHIPK2-NSCs and si-circCon-NSCs were microinjected at 7 d after tMCAO as previously described [18]. At 7 d after tMCAO, the mice were anaesthetized, placed in a stereotactic apparatus and fixed accordingly. The skull was exposed, and a hole was drilled at the appropriate position on the contralateral hemisphere. NSCs (1×10^6) in a total volume of 2 μ L were microinjected into the left lateral ventricle at a rate of 0.1 μ L/min using an infusion pump (RWD, China). The injection coordinates were as follows: anteroposterior, –0.3 mm; lateral, 1.0 mm; and ventral, 2.2 mm.

2.10. In vivo MRI scanning

Mice were anaesthetized with isoflurane (2%) in a mixture of O₂/N₂O (30%/70%) and then imaged with a 7.0 Tesla small animal MR scanner (Bruker PharmaScan, Germany). The infarct volume of mice was assessed by T2-weighted imaging. Their respiration rates were monitored by a Bruker Physiogard system with 30–40 breaths/min. T2-weighted imaging was performed with a 2-dimensional fast-spin

echo sequence (3000/45 ms of repetition time/echo time, 8 average). Sixteen axial slices with a slice thickness of 0.6 mm, a 256 \times 256 matrix and a 20 \times 20 mm field of axial and coronal views were located over the brain, and the olfactory bulb was not included in the field of view. The total scan time was 9 min 36 s, and mice were assessed by T2-weighted images. The hemisphere volume was calculated as follows: \sum hemisphere area \times slice thickness [29]. The lesion volume was acquired based on the high signal area of the T2-weighted images, from which the artefact of brain oedema was subtracted. The lesion volume was calculated as the volume of the contralateral hemisphere minus the ipsilateral non-infarct hemisphere. The infarct volume was calculated using ImageJ software (NIH Image, USA).

2.11. In vivo near-infrared fluorescence imaging (NIF)

Si-circHIPK2-NSCs and si-circCon-NSCs were evaluated at 7, 14, 17, 21 and 28 d after tMCAO by NIF. NIF images were obtained with the Maestro *in vivo* Imaging System (CRi Inc., USA). Near-infrared light was collected with a 540–580 nm bandpass excitation filter and a $>$ 600 nm longpass emission filter.

2.12. Measurement of neurological deficits and behavioural tests

Neurological deficits were assessed 24 h after tMCAO. Neurological function was determined using the modified Neurological Severity Score (mNSS) [29]. The score was graded on a scale of 0 to 14 (normal score, 0; maximum score, 14). One point was awarded for the inability to perform a test or for the lack of a tested reflex; thus, a higher score indicates a more severe injury.

Mice were required to undergo three days of behavioural training prior to tMCAO, and behavioural tests were performed by an independent investigator who was blinded to the experimental group at 3, 7, 14, 21, and 28 d after tMCAO. The adhesive removal test was adopted to assess somatosensory deficits and motor coordination. All mice were placed in a transparent plexiglass box (20 \times 25 \times 32 cm) for the test environment; two adhesive tapes (1 \times 1 cm) were randomly applied with equal pressure to the wrist of each forelimb. The time spent to detect and remove the adhesive was measured. The cylinder test was employed to assess forelimb use asymmetry, and the use of the ipsilateral, contralateral or bilateral forelimbs to explore the cylinder was videotaped for 5 min as previously described [30].

2.13. Immunofluorescence staining

Pretreatment of cells and tissue sections on the coverslips was performed before staining as previously described [29]. Next, the sections and cells were incubated with a mouse anti-GFAP antibody (Cat# 16825-1-AP, RRID:AB_2109646, 1:100, Proteintech), a rabbit anti-TUJ1 antibody (Cat# ab18207, RRID:AB_444319, 1:500, Abcam), an anti-synaptophysin antibody (Cat# ab32127, RRID:AB_2286949, 1:400, Abcam) or an anti-MAP2 antibody (Cat# ab11267, RRID:AB_297885, 1:200, Abcam) or an anti-PSD-95 antibody (Cat# ab2723, RRID:AB_303248, 1:200, Abcam) overnight at 4°C. On the following day, the sections and cells on the coverslips were washed and incubated with Alexa Fluor 488-conjugated anti-mouse IgG (Cat# A-11029, RRID:AB_138404, 1:250, Invitrogen), Alexa Fluor 488-conjugated anti-rabbit IgG (Cat# A-11008, RRID:AB_143165, 1:250, Invitrogen) or Alexa Fluor 594 goat anti-mouse IgG (Cat# A-11005, RRID:AB_141372, 1:250, Invitrogen), Alexa Fluor 594 goat anti-rabbit IgG (Cat# A-11012, RRID:AB_141359, 1:250, Invitrogen) for 1 h. After a final washing step with PBS, the sections were mounted on glass slides, or cells on the coverslips were mounted on glass slides and Prolong gold anti-fade reagent containing DAPI (Southern Biotech, USA) was applied for visualization of nuclei. Immunofluorescence

images were captured by microscopy (Olympus, Japan). TUJ⁺GFP⁺ and GFAP⁺GFP⁺ images were captured using a microscope and z-stack images (Olympus, Japan), and co-localization of TUJ⁺GFP⁺ and GFAP⁺GFP⁺ was calculated as the average of six brain slices in a mice brain using ImageJ software.

2.14. Oxygen and glucose deprivation/reperfusion (OGD/R)

OGD/R treatment was performed as described previously [31]. After 14 d of differentiation, cultured NSCs were exposed to OGD. The cells were rinsed twice with serum- and glucose-free medium and incubated in serum- and glucose-free medium in a hypoxia chamber (Thermo Fisher Scientific, USA). The chamber was flushed with a mixture of 95% N₂ and 5% CO₂ and then sealed and maintained at 37 °C for 2 h. After OGD, the serum-free and glucose-free medium was replaced with normal medium for 6 h of reperfusion, and the cells in the control group were cultured in normal medium for the same incubation times. The pictures were analysed with ImageJ software.

2.15. Golgi-Cox staining

Brains used for Golgi-Cox staining must be fresh and not perfused and fixed [31]. Golgi-Cox staining shows subtle morphological changes in neuronal dendrites and dendritic spines. Golgi-Cox staining was performed using an FD Rapid Golgi Stain Kit (FD Neuro Technologies, USA) according to the user manual. In short, the brains were first placed in the impregnation solution (A + B) for 1 week and then placed in C solution for 1 week. They were then cut into 100 μm coronal sections using a cryostat (Leica, Wetzlar, Germany) and stained. Images of Golgi-stained neurons were acquired on a Olympus microscope (Olympus, Japan). For morphological analysis, 10 random neurons from each sample were measured and the mean was considered the final value of the sample.

2.16. RNA-sequencing analysis

NSCs were transduced with circCon siRNA or circHIPK2 siRNA lentivirus. After 48 h, si-circCon-NSCs and si-circHIPK2-NSCs were collected in TRIzol (Takara, Japan). Total RNA was extracted from the TRIzol, and paired-end sequencing of the final cDNA library (300 ± 50 bp) was performed on an Illumina NovaseqTM 6000 instrument (LC Bio, China) according to the vendor's recommended protocol. RNA-sequencing experiments were performed according to the manufacturer's protocol, and data were analysed by LC Bio. Then, the expression levels of all transcripts were evaluated by calculating the fragments per kilobase per million reads (FPKM). The threshold of significant differential expression was set to $P < 0.05$ and $|\log_2(\text{fold change})| \geq 1$.

2.17. Statistical analysis

Statistical analysis was performed using GraphPad Prism 6 software (La Jolla, USA). All data are presented as the mean ± SEM. Significance was assessed with Student's t-tests for comparisons of 2 groups and One/Two-way ANOVA followed by Holm-Sidak *post hoc* test was used for multi-group comparisons. Behavioral data collected at repeating multiple time points were analyzed using two-way repeated measures ANOVA, followed by Holm-Sidak *post hoc* test. The statistical analyses used for the different experiments are described in the respective figure legends and results were statistically significant if $P < 0.05$ by analysis of variance.

3. Results

3.1. circHIPK2 is involved in the differentiation of NSCs

The dynamic changes of circHIPK2 during the differentiation of NSCs were detected. As shown in Fig. 1a, the expression of circHIPK2 in NSCs was highest at the first day during NSC differentiation and decreased by 50% at 14 d, which suggested that circHIPK2 expression decreased with time during the differentiation of NSCs. To further explore the role of circHIPK2 in the differentiation of NSCs, we first used siRNA lentiviral transduction with circCon or circHIPK2 knock-down constructs. The level of circHIPK2 was significantly decreased in NSCs compared to the control (Fig. 1b). The proliferation of the si-circHIPK2-NSCs suggested that proliferation was not affected compared to that of NSCs transduced with the siRNA circCon (si-circCon-NSCs) under self-renewal conditions, as assessed by BrdU (Fig. 1c-d). Both western blot (Fig. 1e-f) and immunofluorescence staining (Fig. 1g-h) indicated that glial fibrillary acidic protein (GFAP)-positive cells showed no obvious impact compared to the control. However, silencing of circHIPK2 significantly increased the level of TUJ1 compared to the control (Fig. 1e-f), and si-circHIPK2-NSCs generated TUJ1-positive cells at rates 1.9-fold and 2.1-fold higher than those of the control after 7 and 14 d of differentiation, respectively (Fig. 1i-j). As shown in Supplementary Fig. 1, we investigated the expression of the NeuN and MAP2 in the neuronal lineage, and the results indicated that silencing of circHIPK2 in NSCs facilitated NeuN and MAP2 expression. This indicated that silencing of circHIPK2 in NSCs facilitated neuronal differentiation.

Additionally, the findings were further confirmed by overexpressed circHIPK2 in NSCs (Fig. 2a). The circHIPK2-overexpression NSCs (circHIPK2-NSCs) exhibited no changes with proliferation compared with to the circCon-transduced NSCs (circCon-NSCs) by BrdU (Fig. 2b-c). Both western blot (Fig. 2d-e) and immunofluorescence staining (Fig. 2f-g) indicated that GFAP-positive cells had no difference between circHIPK2-NSC group and circCon-NSC group. Interestingly, the proportion of TUJ1 was determined to be significantly reduced in the circHIPK2-NSCs by both western blot (Fig. 2d-e) and immunofluorescence staining (Fig. 2h-i). All the evidences indicated that circHIPK2-NSCs reduced neuronal differentiation.

3.2. Silencing of circHIPK2 expression in NSCs enhances functional recovery after stroke

To determine the effect of si-circHIPK2-NSCs on cerebral infarction volume and functional recovery after stroke, mice were subjected to tMCAO followed by NSC transplantation at 7 d post-tMCAO (Fig. 3a) and for the further processing. Si-circCon-NSCs or si-circHIPK2-NSCs were microinjected into the lateral ventricle of injured mice, and there was no difference in the physiological parameters of the mice in each group before transplantation (Supplementary Table 2). The extent of brain infarct volume was measured by MRI at 1, 7, 14, 21 and 28 d post-tMCAO. As shown in Fig. 3b-c, MRI showed no difference in the infarct size between si-circHIPK2-NSC group and si-circCon-NSC group. Unexpectedly, the neurological deficiency scores were significantly decreased in si-circHIPK2-NSC-transplanted mice compared with si-circCon-NSC-microinjected mice at 21 and 28 d post-tMCAO (Fig. 3d). The similar evidence for a therapeutic effect was also found in the adhesive removal test and cylinder test, with both of which revealed significant differences between si-circHIPK2-NSC-transplanted mice and si-circCon-NSC-transplanted mice at 21 and 28 d post-tMCAO as shown in Fig. 3e-f.

In addition, we further examined the level of circHIPK2 in different organs, including the brain, kidney, lung, spleen, heart and liver using qPCR. As shown in Supplementary Fig. 2a, circHIPK2 was highly expressed in the brain relative to other organs. The expression of circHIPK2 in the ipsilateral cortex of tMCAO mice at different time

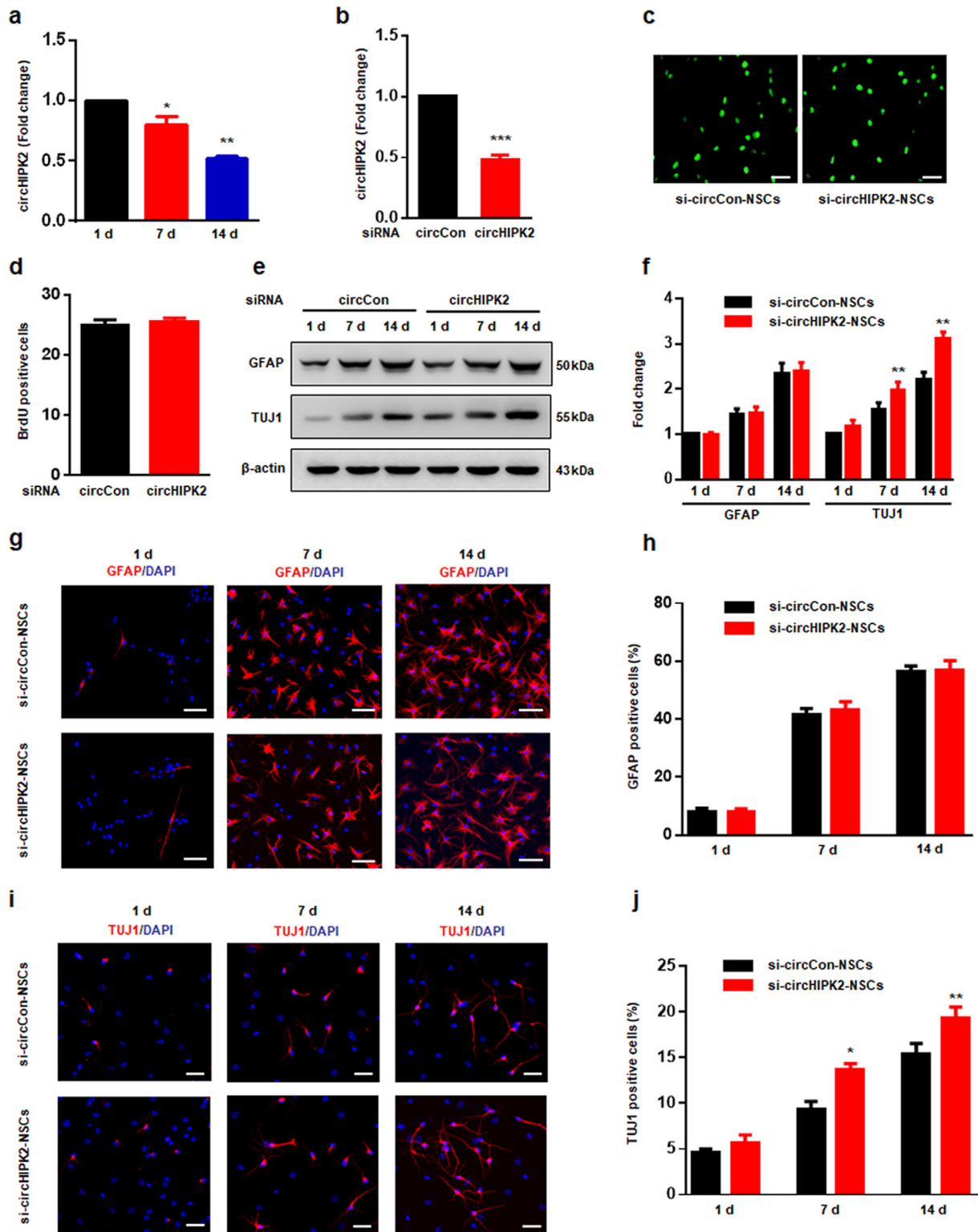


Fig. 1. circHIPK2 is involved in the differentiation of NSCs. (a) qPCR analysis of circHIPK2 expression in NSCs cultured for 1, 7, and 14 d in differentiation medium. All data were presented as mean \pm SEM of 3 independent experiments. * $P < 0.05$, ** $P < 0.01$ vs the 1 d one-way ANOVA followed by Holm-Sidak *post hoc* multiple comparison test. (b) qPCR confirmed that circHIPK2 siRNA lentivirus-transduced NSCs successfully decreased circHIPK2 expression. All data were presented as mean \pm SEM of 3 independent experiments. *** $P < 0.001$ vs the circCon siRNA group using Student's *t*-test. (c-d) Representative image of BrdU immunostaining (c) and quantification of BrdU immunofluorescence-positive cell numbers (d). All data were presented as mean \pm SEM of 3 independent experiments. (e-f) Western blot analysis showing GFAP (astrocyte marker) and TUJ1 (neuronal marker) protein expression in the si-circCon-NSC group and in the si-circHIPK2-NSC group. All data were presented as mean \pm SEM of 3 independent experiments. ** $P < 0.01$ vs the si-circCon-NSCs using two-way ANOVA followed by Holm-Sidak *post hoc* multiple comparison test. (g-j) Representative immunostaining of GFAP⁺ (g) or TUJ1⁺ (i) cells from differentiated NSCs with si-circHIPK2 lentivirus transduction. Scale bar = 50 μ m. Quantification of GFAP⁺ (h) or TUJ1⁺ (j) cell numbers using ImageJ software. Timescale indicates days after NSC differentiation. All data were presented as mean \pm SEM of 3 independent experiments. * $P < 0.05$, ** $P < 0.01$ vs the si-circCon-NSC group cultured in differentiation medium for 7 and 14 d using two-way ANOVA followed by Holm-Sidak *post hoc* multiple comparison test.

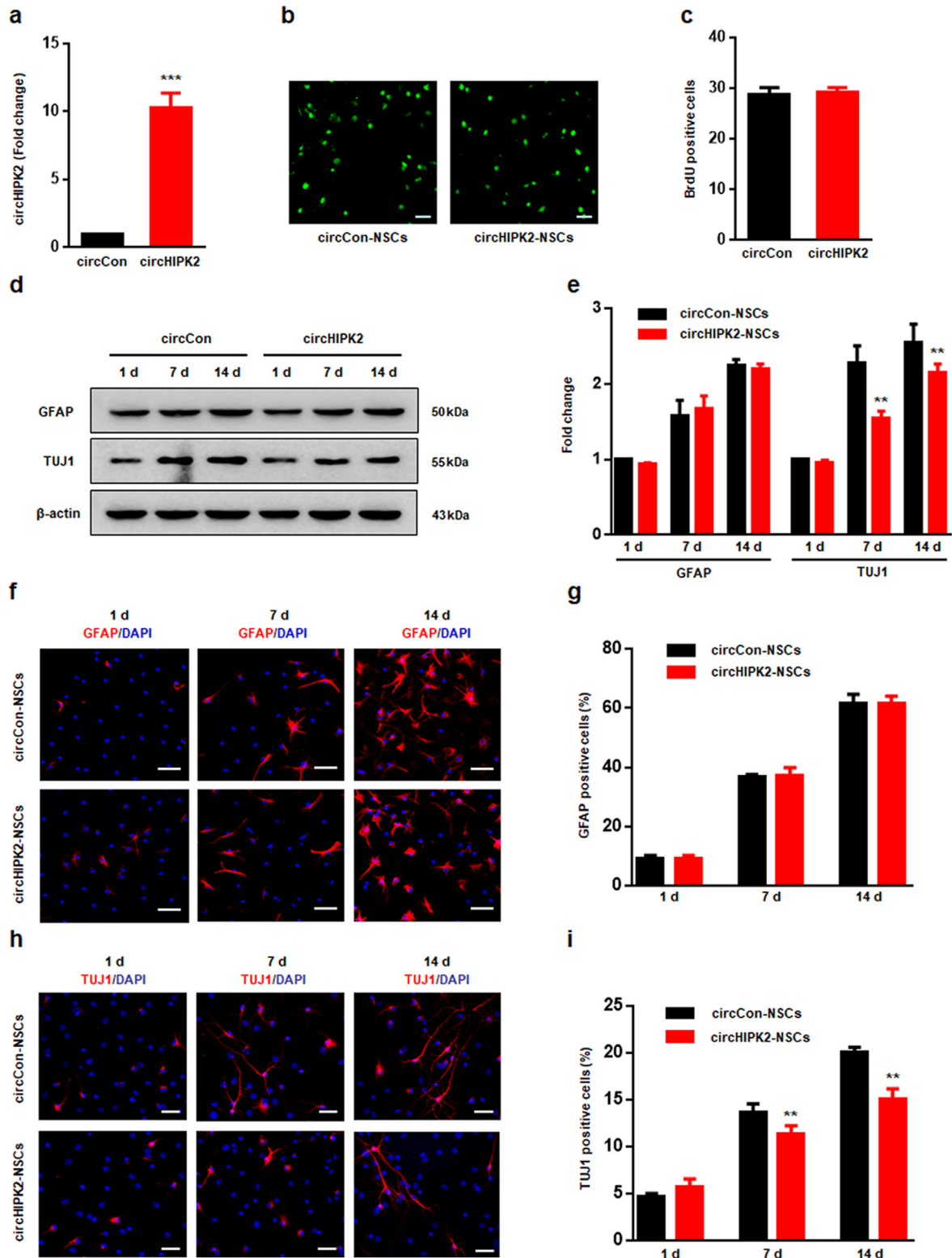


Fig. 2. The overexpression of circHIPK2 suppresses the differentiation of NSCs. (a) qPCR confirmed that the overexpression of circHIPK2 lentivirus-transduced NSCs successfully increased circHIPK2 expression. All data were presented as mean \pm SEM of 3 independent experiments. ^{***} $P < 0.001$ vs the circCon-NSC group using Student's *t*-test. (b-c) Representative of BrdU immunostaining (b) and quantification of BrdU immunofluorescence-positive cell numbers (c). All data were presented as mean \pm SEM of 3 independent experiments. (d-e) Western blot analysis showing GFAP and TUJ1 protein expression in the circCon-NSC group and in the circHIPK2-NSC group. All data were presented as mean \pm SEM of 3 independent experiments. ^{**} $P < 0.01$ vs the si-circCon-NSC group cultured in differentiation medium for 7 and 14 d using two-way ANOVA followed by Holm-Sidak *post hoc* multiple comparison test. (f-i) Representative immunostaining of GFAP⁺ (f) or TUJ1⁺ (h) cells from differentiated NSCs with circHIPK2 lentivirus transduction. Scale bar = 50 μ m. Quantification of GFAP⁺ (g) or TUJ1⁺ (i) cell numbers using ImageJ software. The timescale indicates days after NSC differentiation. All data were presented as mean \pm SEM of 3 independent experiments. ^{**} $P < 0.01$ vs the circCon-NSC group cultured in differentiation medium for 7 and 14 d using two-way ANOVA followed by Holm-Sidak *post hoc* multiple comparison test.

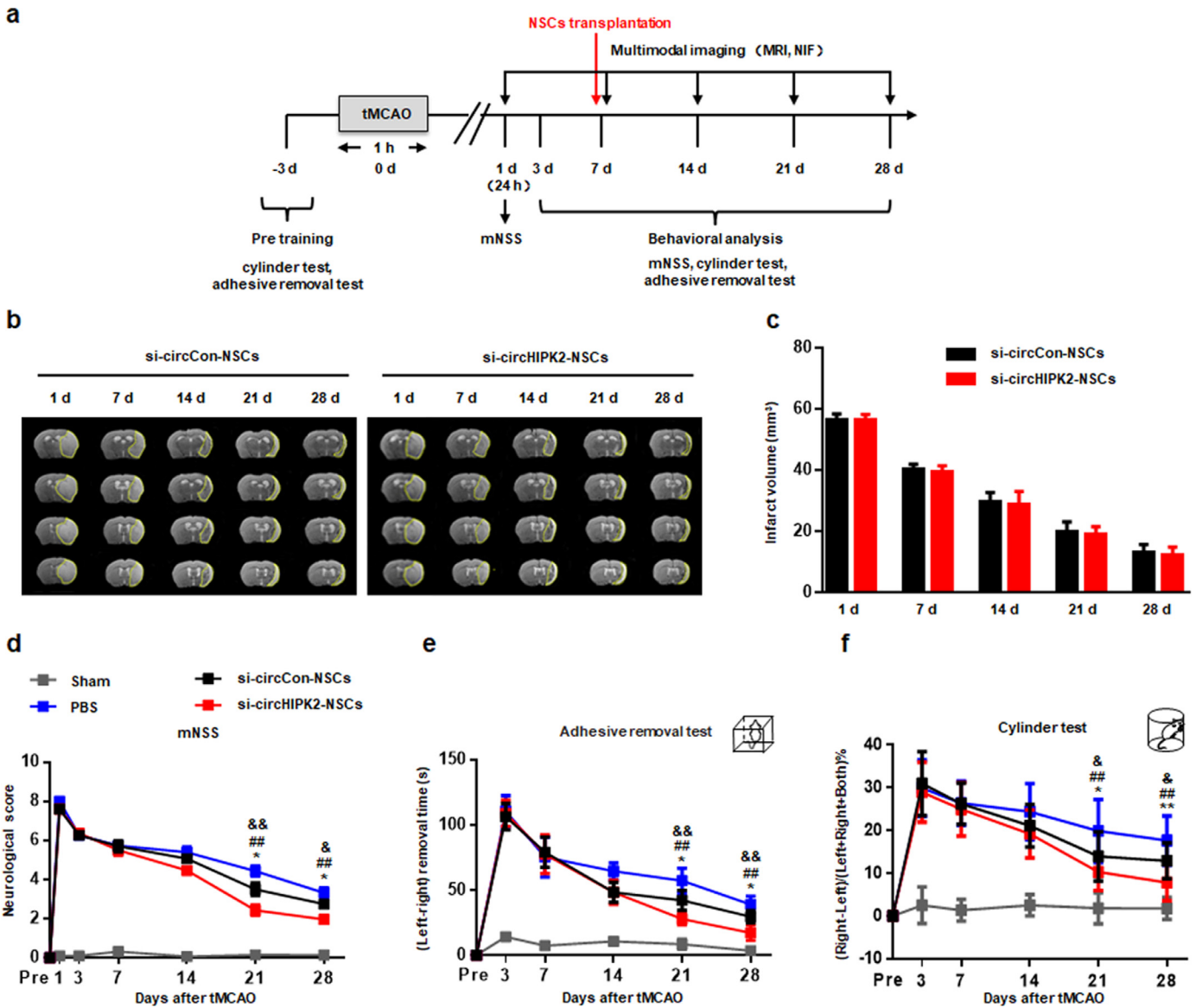


Fig. 3. Silencing of circHIPK2 expression in NSCs enhances functional recovery after stroke. (a) Illustration of the experimental procedure. (b–c) T2-weighted MRI was used to confirm the presence of ischaemic stroke before and after transplantation. The dashed line denotes the infarct area. $n = 11$ mice per group. (d) Neurological deficits were measured by mNSS at 1, 3, 7, 14, 21, and 28 d after tMCAO. (e–f) The adhesive removal tests (e) and cylinder tests of forelimb symmetry (f) were performed at 3, 7, 14, 21, and 28 d after tMCAO. $n = 14$ mice in the sham group, $n = 14$ in the PBS-microinjected tMCAO (PBS) group, $n = 14$ in the si-circCon-NSC-microinjected tMCAO (si-circCon-NSCs) group and $n = 14$ in the si-circHIPK2-NSC-microinjected tMCAO (si-circHIPK2-NSCs) group. Mean \pm SEM; * $P < 0.05$, ** $P < 0.01$, the si-circCon-NSC group vs the PBS group; # $P < 0.05$, ## $P < 0.01$, the si-circHIPK2-NSC group vs the PBS group; & $p < 0.05$, && $p < 0.01$, the si-circCon-NSC group vs the si-circHIPK2-NSC group (two-way repeated-measures ANOVA followed by Holm-Sidak *post hoc* multiple-comparison tests).

points was also detected. As shown in Supplementary Fig. 2b, the expression level of circHIPK2 remained unchanged in the tMCAO mice. Taken together, these findings suggest the substantial post-stroke repair potential of si-circHIPK2-NSC therapy, which protects against brain damage without affecting infarct size and promotes functional recovery.

3.3. Distribution of the transplanted NSCs in tMCAO mice

Having determined the role of si-circHIPK2-NSCs in functional recovery, we next sought to examine whether si-circHIPK2-NSCs recolonize and reach to the ipsilateral hemisphere. NSCs from EGFP transgenic mice were isolated from the embryonic hippocampus (Fig. 4a). After transduction with circCon or circHIPK2 siRNA lentivirus, si-circCon-NSCs and si-circHIPK2-NSCs were microinjected at 7 d after tMCAO and tracked longitudinally *in vivo* by NIF of the

endogenous fluorescent signal. NIF showed a progressive decline in the fluorescent signal in both groups, from 100% to 25% within 3 weeks of transplantation. Although there was a tendency that the brain fluorescence intensity in si-circHIPK2-NSC group was higher than si-circCon-NSC group, the difference was not statistical (Fig. 4b–c). These results suggested that transplanted NSCs gradually migrated to the infarct side, while the fluorescent signal of mice showed a time-dependent decrease. *Ex vivo* images of mice brains were assessed to further evaluate the possibility of transplanting NSCs to the infarct brain regions. As shown in Fig. 4d–e, the transplanted NSCs migrated to the infarct regions and the fluorescence intensity was gradually weak from 7 d to 28 d after tMCAO. In addition, the fluorescence intensity and the distribution profile did not show remarkable differences between si-circCon-NSCs and si-circHIPK2-NSCs. After 28 d of tMCAO, frozen sections of the mouse brain with DAPI staining were pictured by electron microscope to identify NSCs at the injection

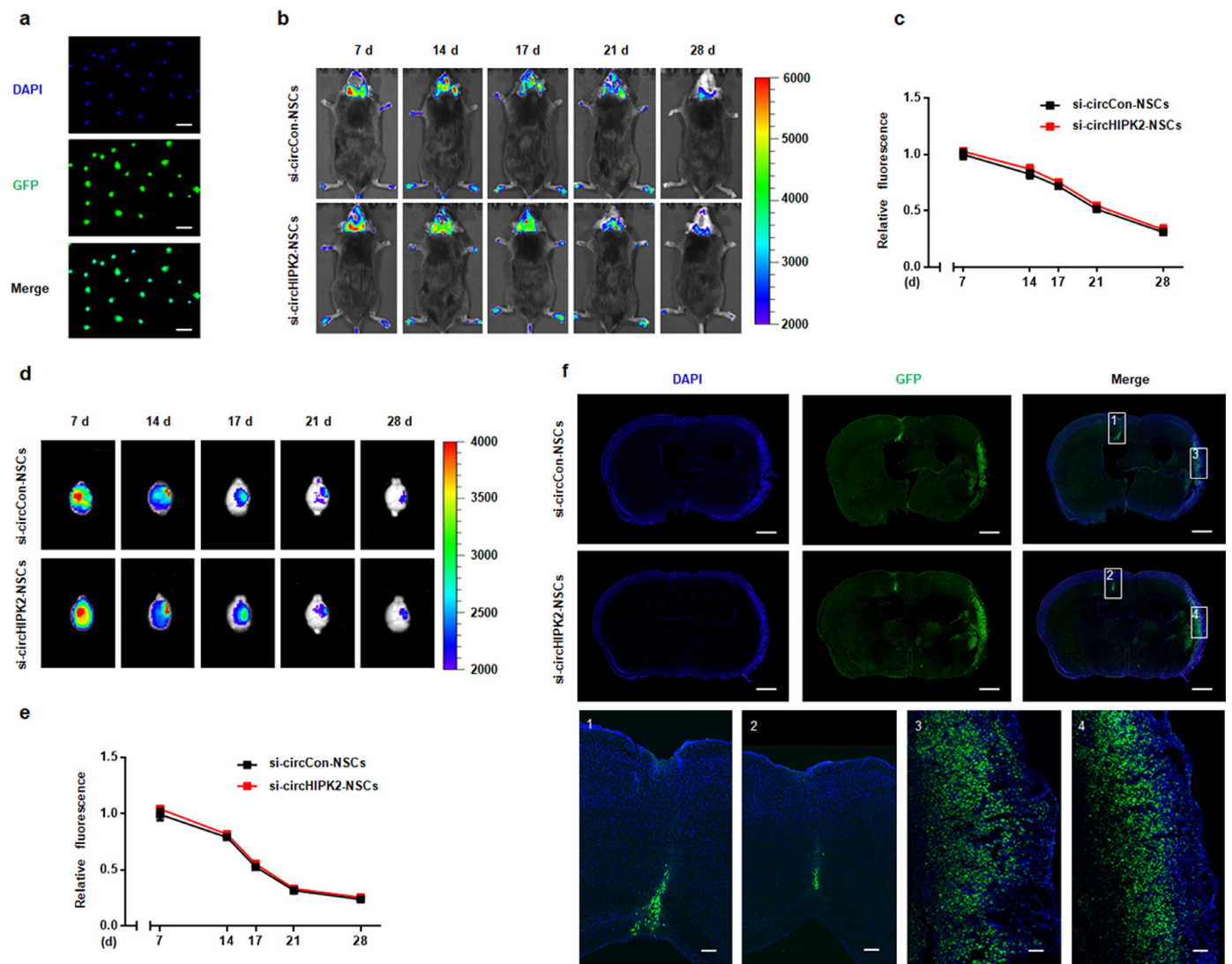


Fig. 4. Distribution of the transplanted NSCs in tMCAO mice. (a) Representative images of the GFP-positive NSCs from transgenic EGFP mice. Scale bar = 50 μ m. (b-c) NIF of the mouse brain at 7, 14, 17, 21, and 28 d after tMCAO and quantification of the fluorescence signal from engrafted si-circCon-NSCs and si-circHIPK2-NSCs. $n = 5$ per group. (d-e) NIF of ex vivo mouse brain at 7, 14, 17, 21, and 28 d after tMCAO and quantification of the fluorescence signal from engrafted si-circCon-NSCs and si-circHIPK2-NSCs. $n = 5$ per group. (f) Immunofluorescence evaluation of mouse brains implanted with NSCs. Scale bar = 200 μ m. DAPI (blue), nucleus; GFP (green), NSCs; $n = 5$ per group. Mean \pm SEM. (For interpretation of the references to color in this figure legend, the reader is referred to the web version of this article.)

site and in the ischaemic area (Fig. 4f). The fluorescence demonstrated that huge number of GFP-positive cells migrated from the injection site to the infarcted cortex. Massive infiltration of GFP-active cells was detected in the ischaemic territory in proximity to necrotic tissue areas (Fig. 4f). This finding convincingly demonstrated that the NSCs migrated across the corpus callosum into the lesioned tissue.

3.4. Silencing of circHIPK2 enhances NSC-differentiated neurons and promotes neuronal plasticity in vitro

The increased functional recovery of injured mice combined with the recolonization of transplanted si-circHIPK2-NSCs urged us to ascertain whether si-circHIPK2-NSCs implicated in ischaemic-induced structural alterations of neurons. We subjected neurons that differentiated from NSCs to OGD/R. OGD/R exposure significantly decreased the total process length and dendrite spine density of surviving neurons, and si-circHIPK2 ameliorated the process length (Fig. 5a-b). Similarly, OGD/R exposure led to a significant decrease in dendritic spine density, which was ameliorated by si-circHIPK2 (Fig. 5c-d). The findings were further confirmed by western blot

analysis. The expression of synaptophysin, PSD-95 and TUJ1 decreased significantly under OGD/R, and this change was reversed by si-circHIPK2 treatment (Fig. 5e-f). Furthermore, silencing circHIPK2 had no obvious effect on the astrocyte size and GFAP expression against OGD/R (Supplementary Fig. 3). Therefore, silencing circHIPK2 enhances the differentiation of NSCs to neurons and promotes neuronal plasticity against OGD/R.

3.5. Si-circHIPK2 triggers NSC-differentiated neurons and facilitates neuronal plasticity in tMCAO mice

To investigate whether the si-circHIPK2-NSCs were capable of differentiating into neuronal cells *in vivo*, double immunostaining of TUJ1 (neuronal maker) and GFP (transplanted NSCs) in the ischaemic site was conducted at 28 d post-tMCAO. In addition to the endogenous neurons, the NSCs homing to the ischaemic site exhibited TUJ1-positive and visualized as highlighted red spots in the immunostaining photomicrograph. As shown in Fig. 6a-c, the number of TUJ1⁺GFP⁺ co-labelled neuronal cells in the si-circHIPK2-NSC group was significantly higher than that in the si-circCon-NSC group, which indicated that silencing of circHIPK2 triggered neuronal differentiation of NSCs.

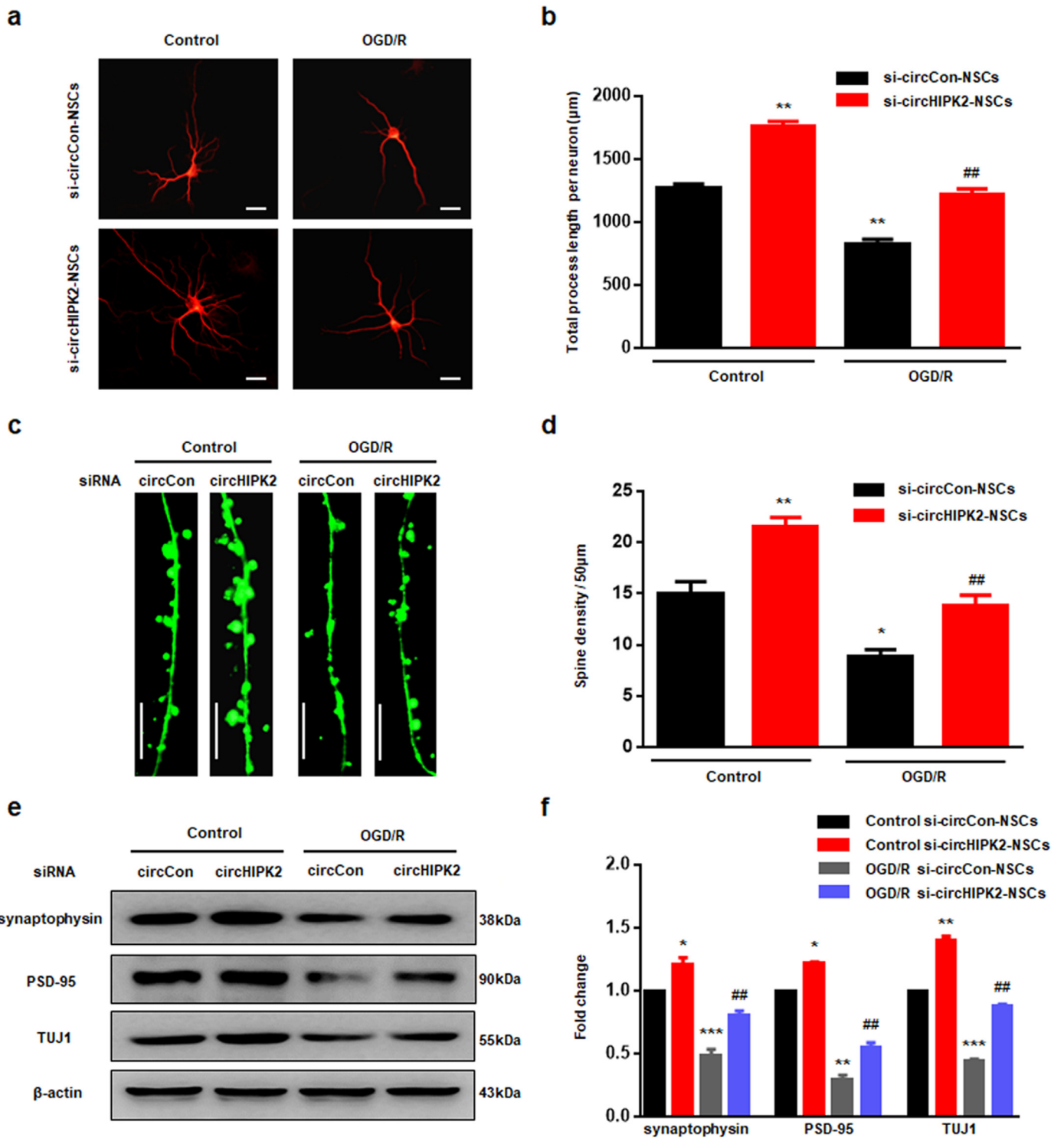


Fig. 5. Silencing of circHIPK2 enhances NSC-differentiated neurons and promotes neuronal plasticity *in vitro*. (a-b) Images showing representative neurons differentiated from NSCs and bar graphs showing the total process length per neuron. Scale bar = 50 µm. Six neurons were measured in each biological sample. ** $P < 0.01$ vs the control si-circCon-NSC; ## $P < 0.01$ vs the OGD/R-treated si-circCon-NSC group using two-way ANOVA followed by Holm-Sidak *post hoc* multiple-comparison tests. (c-d) Images and bar graph showing the dendrite spine density of representative neurons differentiated from NSCs. Six neurons were measured in each biological sample. Scale bar = 10 µm. * $P < 0.05$, ** $P < 0.01$ vs the control si-circCon-NSC; ## $P < 0.01$ vs the OGD/R-treated si-circCon-NSC group using two-way ANOVA followed by Holm-Sidak *post hoc* multiple-comparison tests. (e-f) Neurons differentiated from si-circHIPK2-NSCs attenuated the OGD/R-induced decreases in synaptophysin, PSD-95 and TUJ1. All data were presented as mean ± SEM of 4 independent experiments. * $P < 0.05$, ** $P < 0.01$, *** $P < 0.001$ vs the control si-circCon-NSC group; ## $P < 0.01$ vs the OGD/R-treated si-circCon-NSC group using two-way ANOVA followed by Holm-Sidak *post hoc* multiple-comparison tests.

In addition, si-circHIPK2 treatment did not influence the differentiation of NSCs into astrocyte-like cells or the percentage of GFAP-positive cells at different time points after tMCAO (Supplementary Fig. 4). The *in vivo* findings suggested that functional recovery was causally

associated with circHIPK2-mediated neuronal production from grafted NSCs.

Staining for synaptic markers demonstrated a higher number of colocalized presynaptic (synaptophysin) and postsynaptic (PSD-95)

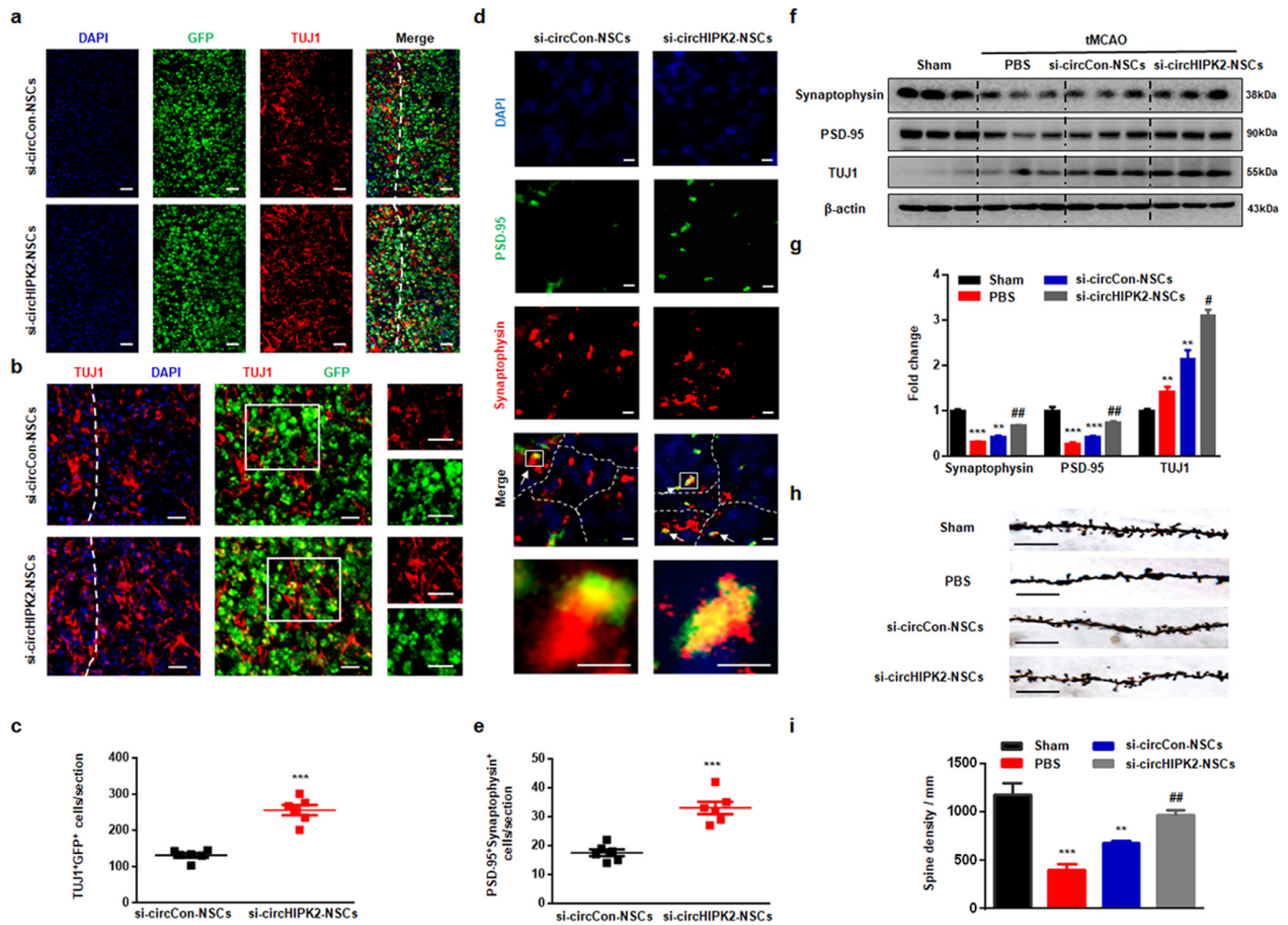


Fig. 6. Si-cirHIPK2 triggers NSC-differentiated neurons and facilitates neuronal plasticity in tMCAO mice. (a) Representative immunofluorescence images of mouse cerebral infarction regions 28 d after tMCAO showing TUJ1 (red; neuronal marker) and GFP (green, NSCs) coimmunostaining in mice treated with si-circCon-NSCs and si-cirHIPK2-NSCs. DAPI (blue), cell nuclear staining. Scale bar = 100 μm . $n = 6$ mice per group. (b) TUJ1⁺GFP⁺ double-positive cells from the mouse cerebral infarction region 28 d after tMCAO and si-circCon-NSCs (left) or si-cirHIPK2-NSCs (right). Insets, individual channels from the boxed regions. Scale bar = 20 μm . (c) Scatter plot of TUJ1⁺GFP⁺ double-positive cells 28 d after tMCAO. $n = 6$ mice per group. $***P < 0.001$ vs the si-circCon-NSC group using Student's *t*-test. (d) Synaptophysin (red) and PSD-95 (green) coimmunostaining in mice treated with si-circCon-NSCs and si-cirHIPK2-NSCs. Arrows, colocalized puncta. Insets, high magnification of boxed regions showing colocalized puncta. DAPI (blue), nuclear staining; scale bar = 50 μm (main images), 10 μm (insets). Dashed lines, borders between NSCs. (e) Scatter plot of synaptophysin and PSD-95 colocalized puncta in the mouse cerebral infarction region 28 d after tMCAO. $n = 6$ mice per group. $***P < 0.001$ vs the si-circCon-NSC group using Student's *t*-test. (f-g) Western blot analysis of synaptophysin, PSD-95 and TUJ1 expression in the ischaemic cortex 28 d after tMCAO. $n = 6$ mice per group. $***P < 0.01$, $***P < 0.001$ vs the sham group; $##P < 0.01$ vs the si-circCon-NSC group using two-way ANOVA followed by Holm-Sidak *post hoc* multiple-comparison tests. (h-i) Representative images and bar graph showing dendritic spine density in the peri-infarct cortex 28 d after tMCAO. Six neurons were measured in each biological sample. Scale bar = 10 μm . $**P < 0.01$, $***P < 0.001$ vs the sham group; $##P < 0.01$ vs the si-circCon-NSC group using two-way ANOVA followed by Holm-Sidak *post hoc* multiple-comparison tests. (For interpretation of the references to color in this figure legend, the reader is referred to the web version of this article.)

puncta on the engrafted GFP⁺ NSCs in si-cirHIPK2-NSC-treated mice relative to si-circCon-NSC-treated mice. Quantitative analysis revealed a 3-fold increase in these putative contacts in si-cirHIPK2-NSC-treated mice relative to si-circCon-NSC-treated mice (Fig. 6d-e), which suggested the formation of synapses. Moreover, the levels of synaptophysin, PSD-95 and TUJ1 were decreased in the si-circCon-NSC-treated group and significantly alleviated by si-cirHIPK2-NSC treatment, as determined by western blot (Fig. 6f-g). Consistent with evidence for behavioural improvement, tMCAO treatment significantly decreased the spine numbers in the peri-infarct cortex of mice at 28 d post-tMCAO, which was ameliorated by si-cirHIPK2-NSC treatment (Fig. 6h-i). The above results suggest that si-cirHIPK2-NSCs could facilitate neural plasticity in tMCAO mice.

3.6. Silencing of *circHIPK2* promotes NSC differentiation via downstream *SMOX*

To explore the mechanism underlying si-cirHIPK2-NSC-induced neuroprotection, regeneration and functional recovery after

ischaemic stroke, we next sought for candidate target genes. The mRNA expression profiles of si-circCon-NSCs and si-cirHIPK2-NSCs were obtained using RNA sequencing (GEO accession number: GSE133701). A total of 4 upregulated genes and 16 downregulated genes were determined with cutoffs of $|\log_2(\text{fold change})| \geq 1$ and adjusted *P* value < 0.05 (Fig. 7a). Among these 20 genes which had the most significant differences on expression in si-circCon-NSCs and si-cirHIPK2-NSCs, 4 upregulated genes (Supplementary Fig. 5a) and 16 downregulated genes (Supplementary Fig. 5b and 7b) were further verified by qPCR. Among these, the expression levels of 4 genes were confirmed the same trends with the RNA sequencing results. And in the 4 genes, spermine oxidase (*Smox*) is an important mediator involved in the regulation of cerebral ischaemic injury [32]. Of course, we can't rule out the potential role of the 3 other genes in cerebral ischaemic injury.

Both the mRNA and protein levels of *Smox* were dramatically decreased in si-cirHIPK2-NSCs (Fig. 7b-d), confirming the results of RNA sequencing. Silencing of *circHIPK2* significantly inhibited the

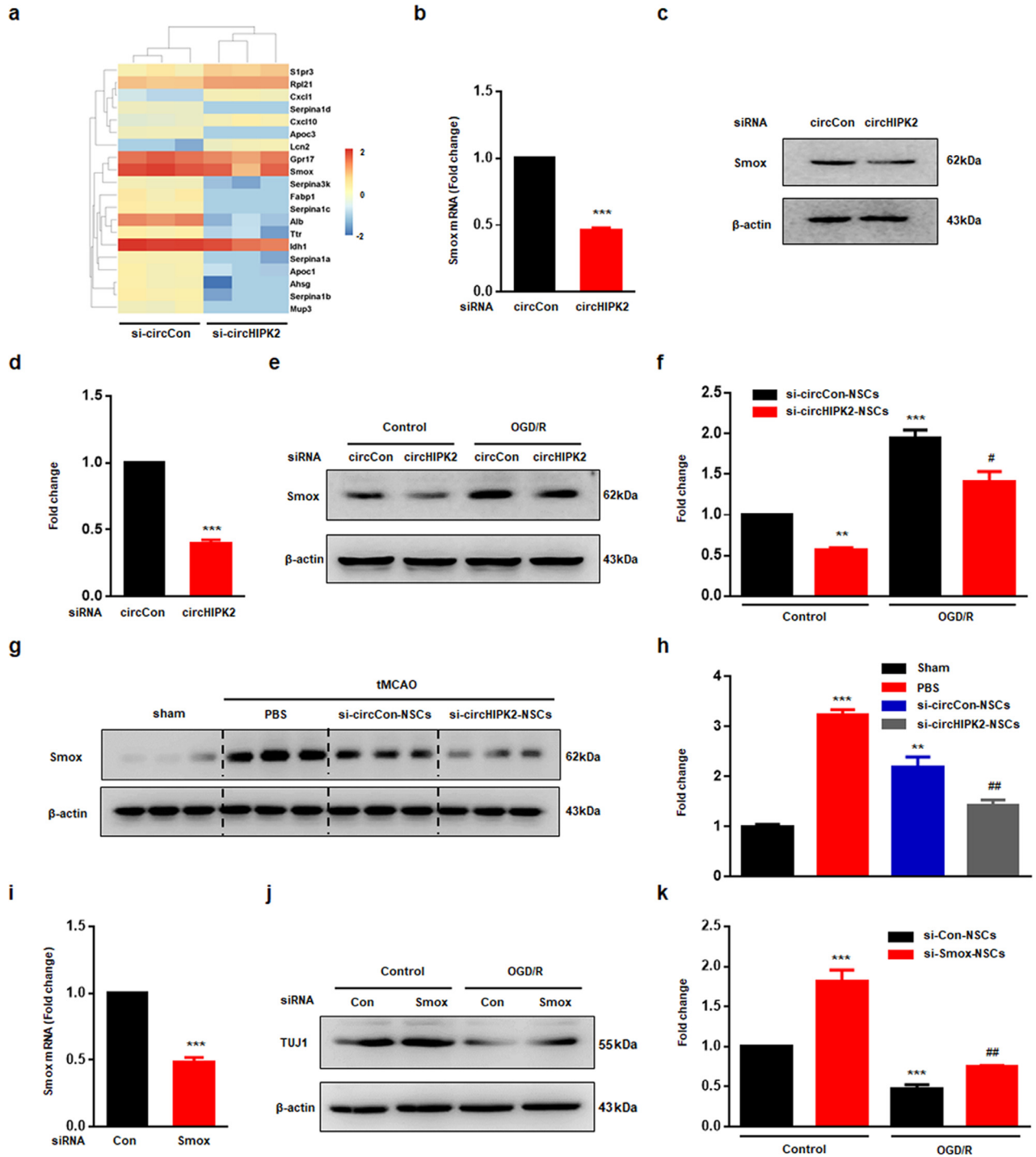


Fig. 7. Silencing of circHIPK2 promotes NSC differentiation via Smox. (a) Heatmap assessing the variations in mRNA expression between the si-circCon-NSC group and the si-circHIPK2-NSC group. $n = 3$ per group. $^*P < 0.05$ vs the si-circCon-NSC group. (b) The level of Smox mRNA in circHIPK2 siRNA transduced NSCs analysed by qPCR. All data were presented as mean \pm SEM of 3 independent experiments. $^{***}P < 0.001$ vs the circCon siRNA group using Student's *t*-test. (c-d) Western blot analysis of Smox expression in circHIPK2 siRNA transduced NSCs. All data were presented as mean \pm SEM of 3 independent experiments. $^{***}P < 0.001$ vs the circCon siRNA group using Student's *t*-test. (e-f) circHIPK2 siRNA attenuated the expression of OGD/R-induced Smox expression in NSCs, as determined by western blot analysis. NSCs were treated with OGD for 2 h and reperused for 6 h. All data were presented as mean \pm SEM of 3 independent experiments. $^{**}P < 0.01$, $^{***}P < 0.001$ vs the control si-circCon group; $^*P < 0.05$ vs the OGD/R-treated si-circCon group using two-way ANOVA followed by Holm-Sidak *post hoc* multiple-comparison tests. (g-h) Western blot analysis of Smox expression in tMCAO mice injected with si-circCon-NSCs and si-circHIPK2-NSCs. $n = 6$ per group. $^{**}P < 0.01$, $^{***}P < 0.001$ vs the sham group; $^{##}P < 0.01$ vs the si-circCon-NSC group using two-way ANOVA followed by Holm-Sidak *post hoc* multiple-comparison tests. (i) qPCR analysis of Smox mRNA in the si-Con-NSC group and si-Smox-NSC group. All data were presented as mean \pm SEM of 3 independent experiments. $^{***}P < 0.001$ vs the si-Con-NSC group. (j-k) Smox siRNA attenuated the expression of OGD/R-induced TUJ1 in NSCs determined by western blot. All data were presented as mean \pm SEM of 3 independent experiments. $^{***}P < 0.001$ vs the si-Con-NSC group; $^{##}P < 0.01$ vs the OGD/R si-Con group using two-way ANOVA followed by Holm-Sidak *post hoc* multiple-comparison tests.

increased expression of Smox induced by OGD/R (Fig. 7e–f). Similarly, we found that si-circHIPK2-NSCs significantly reduced the increased expression of Smox in ischaemic tissue (Fig. 7g–h). Mechanically, to further verify that Smox acts as a mediator to regulate the expression of TUJ1, NSCs were transfected with Smox siRNA. Knockdown of Smox efficiently decreased the expression of Smox (Fig. 7i) and significantly promoted the TUJ1 expression induced by OGD/R (Fig. 7j–k). Overall, it was confirmed that knockdown of Smox could promote the differentiation of NSCs, increase the number of differentiated neurons and improve neural plasticity.

4. Discussion

CircRNAs are endogenous, conserved in mammalian cells and relatively abundant [33]. They have been reported to be involved in a variety of CNS diseases, such as Alzheimer's disease, glioma, drug abuse and ischaemic stroke [20,34–37]. Recently, studies have indicated that circRNAs are closely related to neuronal development, as evidenced by their specific distribution in different brain regions and developmental stages [17,38].

Our preliminary study found that there is a binding site between circHIPK2 and miR-124 [20], and miR-124 was reported to not only be involved in the regulation of stem cell differentiation but also to promote the number of NSC-differentiated neurons [39,40]. Other researchers found that miR-124 can play a neuroprotective role and promote nerve recovery after stroke [41]. Given its great potential to repair damaged regions and extend the therapeutic time window for intervention, NSC transplantation is a novel therapeutic approach that can benefit more stroke patients [4,5]. Therefore, we wanted to investigate whether circHIPK2 is also involved in the differentiation and regulation of NSCs and elucidate its potential role in ischaemic stroke. Moreover, to rule out the effect of lentivirus on NSC proliferation and differentiation, we also confirmed that lentivirus-transduced NSCs did not affect NSC proliferation and differentiation *in vivo* and *in vitro* by western blot and immunostaining experiments (Supplementary Fig. 6). Additionally, we also examined the effects of NSC transduction with lentivirus on neural plasticity and downstream proteins, and the results showed that lentivirus-transduced NSCs did not affect the neural plasticity and the Smox expression (Supplementary Fig. 7).

The expression level of circHIPK2 decreased with time during the differentiation of NSCs, and silencing of circHIPK2 in NSCs facilitated neuronal differentiation. Previous assessment of NSC-based therapies in animal models of stroke has commonly used direct intracerebral administration of stem cells [6,7]. In our study, transplanted NSCs provided long-lasting neuroprotection, which was indicated by enhanced functional recovery. The fate, homing and function of transplanted NSCs *in vivo* have always been key issues in stem cell therapy. Therefore, a variety of methods were used to trace the transplanted NSCs. We found that NSCs migrated to the infarcted hemisphere of tMCAO animals, indicating that these cells homed to the damaged areas of the brain. This is consistent with previous studies showing that NSCs are able to use endogenous adhesion and chemo-attractant molecules to extravasate from the vascular compartment and migrate to the ischaemic lesion [8,42,43].

In this study, NSCs were microinjected into the left lateral ventricle at 7 d after tMCAO. The selected scheme also considered the potential clinical application of NSCs. According to the clinical course of stroke patients [44], the possibility of using stem cell therapy in the acute phase of stroke is low. Transplantation of NSCs at earlier time points (6–24 h after stroke) leads to greater differentiation into astrocytes, whereas transplantation at later time points (7–14 d after stroke) leads to greater differentiation into neurons [8]. Previous work has shown that the acute release of products related to tissue damage and death typically subsides within 7 d post-tMCAO, thus providing a potentially less hostile graft environment as well as reduced brain injury,

inflammation, and both short- and long-term functional deficits [7]. Stem cell transplantation at delayed time points (e.g., 7 d after stroke) in rodent models can avoid the cytotoxic environment in the acute phase of MCAO [45,46]. Thus, NSC transplantation during the chronic phase of stroke may be an attractive method of repairing the damaged brain. We assessed the potential of NSCs for modulating repair processes and facilitating functional recovery when transplanted 7 d after tMCAO and observed improved sensorimotor recovery. Therefore, the present study also provides important experimental data for further applications of NSCs in stroke.

We analysed the biodistribution of si-circHIPK2-NSCs in the damaged hemisphere, and their effects on brain neuroplasticity. Previous studies indicated that ischaemic stroke occurs when an artery supplying the brain becomes occluded, leading to diverse pathophysiological changes including brain edema, neuronal cell death, and synapse loss in the brain [47]. Cerebral ischaemia suppresses the expression of synaptophysin and PSD-95, which are important in modulating synaptogenesis. Interestingly, overexpression of PSD-95 increases the number and size of spines. Spine growth and stabilization require activity-dependent PSD-95 expression and local translational activity [48–50]. In addition, researchers found that the reduction in synaptophysin can reduce synaptic plasticity in the brain [51]. Moreover, researchers not only demonstrated a correlation between changes in brain function and plasticity after stroke but also found that increased brain plasticity usually has a positive effect on recovery of motor function after stroke [30,52]. Similar to our findings, si-circHIPK2-NSCs promoted functional recovery and neural plasticity after stroke.

When brain damage such as cerebral ischaemia occurs, astrocytes initiate an emergency rescue mode and rapidly proliferate in the ischaemia area. At this point, the resting astrocytes transform into activated astrocyte cells that can self-divide like stem cells, rapidly accumulate in the core edge of damaged brain tissue, such as that occurring with ischaemia, and perform brain repair functions [53]. Studies have reported that a decrease in gliosis is related to a reduction in the infarct size [30]. Therefore, the elimination of glial scars caused by glial cells is also a major problem in the repair of brain injury. Our study found that there was no significant reduction in the formation of glial scars after treatment with si-circHIPK2-NSCs for the repair of brain injury.

Smox, a member of the polyamine oxidases [54], has been shown to be involved in ischaemic brain damage [32] and was increased in the plasma of stroke patients [55]. Moreover, overexpression of Smox in the neocortex resulted in higher H₂O₂ production and glial activation. Smox activity occurred both in the cytoplasm and the nucleus [56,57], and its production of H₂O₂ in close proximity to DNA results in oxidative DNA damage that elevates the potential for neoplastic transformation [58]. We found that Smox can regulate NSC differentiation. This study represents the first report showing that Smox acts as an important downstream mediator of circHIPK2 and can regulate the level of TUJ1 in differentiated neurons of NSCs induced by OGD/R. After treatment with si-circHIPK2-NSCs, the level of Smox significantly decreased in the ischaemic tissue of tMCAO mice. Our findings seem consistent with those of a previous study that showed that Smox downregulation significantly improved tMCAO-induced brain injury as evidenced by ameliorated neurological deficits [32]. The detailed mechanism of Smox in NSC differentiation needs to be further examined in future studies.

In summary, this study explored the potential of si-circHIPK2-NSCs as a neuroprotective therapy for ischaemic stroke in a mouse model for the first time. Given the lack of current treatments and the narrow therapeutic window for t-PA, si-circHIPK2-NSCs have shown promising beneficial effects after stroke, and the results are quite encouraging. This study marks the first time that Smox has been demonstrated to act as an important downstream mediator of circHIPK2 and has been shown to regulate the level of TUJ1 in differentiated neurons of NSCs induced by OGD/R. In addition, the expression level of Smox was significantly decreased in the ischaemic tissues of

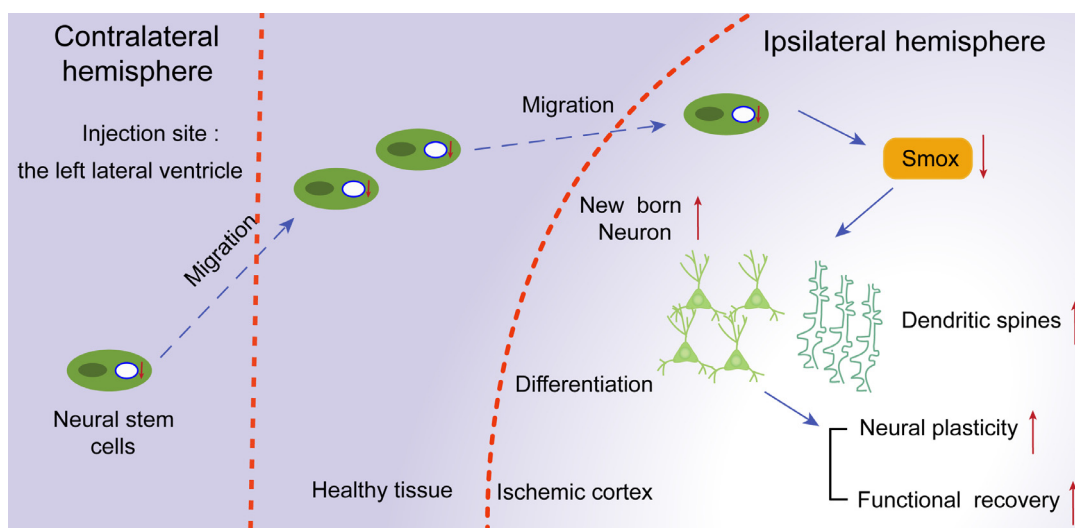


Fig. 8. Si-circHIPK2-NSCs enhance functional recovery by facilitating neuronal differentiation via Smox. Transplanted NSCs in the contralateral hemisphere migrate to the ipsilateral hemisphere, where silencing of circHIPK2 in NSCs facilitates neuronal differentiation via downstream inhibition of Smox expression, with subsequent enhancement of neural plasticity and functional recovery after stroke.

tMCAO mice. Moreover, our study reported the improvement of functional recovery and brain plasticity after stroke, revealing the potential of si-circHIPK2-NSCs as a promising treatment for ischaemic stroke (Fig. 8).

Declaration of Competing Interest

The authors have no competing interests to declare.

Acknowledgments and funding sources

This work was funded by the National Key Research and Development Program of China (no. 2017YFA0104303), the International Cooperation and Exchange of the National Natural Science Foundation of China (no. 81761138048), the National Natural Science Foundation of China (no. 81673410), the Jiangsu Innovation & Entrepreneurship Team Program to H.Yao, the National Natural Science Foundation of China (nos. 81603090 and 81973304) to Y. Zhang. The funders had no role in study design, data collection, data analysis, interpretation, writing of the manuscript.

Supplementary materials

Supplementary material associated with this article can be found in the online version at doi:10.1016/j.ebiom.2020.102660.

References

- Benjamin EJ, Blaha MJ, Chiuve SE, et al. Heart disease and stroke statistics-2017 update: a report from the American heart association. *Circulation* 2017;135:e146–603.
- Schwamm LH, Ali SF, Reeves MJ, et al. Temporal trends in patient characteristics and treatment with intravenous thrombolysis among acute ischemic stroke patients at get with the guidelines-stroke hospitals. *Circ Cardiovasc Qual Outcomes* 2013;6:543–9.
- Wei L, Wei ZZ, Jiang MQ, Mohamad O, Yu SP. Stem cell transplantation therapy for multifaceted therapeutic benefits after stroke. *Prog Neurobiol* 2017;157:49–78.
- Vieira MS, Santos AK, Vasconcelos R, et al. Neural stem cell differentiation into mature neurons: mechanisms of regulation and biotechnological applications. *Biotechnol Adv* 2018;36:1946–70.
- Hess DC, Borlongan CV. Cell-based therapy in ischemic stroke. *Expert Rev Neurother* 2008;8:1193–201.
- Smith EJ, Stroemer RP, Gorenkova N, et al. Implantation site and lesion topology determine efficacy of a human neural stem cell line in a rat model of chronic stroke. *Stem Cells* 2012;30:785–96.
- Wang Y, Zhao Z, Rege SV, et al. 3K3A-activated protein C stimulates postischemic neuronal repair by human neural stem cells in mice. *Nat Med* 2016;22:1050–5.
- Rosenblum S, Wang N, Smith TN, et al. Timing of intra-arterial neural stem cell transplantation after hypoxia-ischemia influences cell engraftment, survival, and differentiation. *Stroke* 2012;43:1624–31.
- Broughton BR, Reutens DC, Sobey CG. Apoptotic mechanisms after cerebral ischemia. *Stroke* 2009;40:e331–9.
- Fann DY, Lee SY, Manzanero S, Chunduri P, Sobey CG, Arumugam TV. Pathogenesis of acute stroke and the role of inflammasomes. *Ageing Res Rev* 2013;12:941–66.
- Martino G, Pluchino S, Bonfanti L, Schwartz M. Brain regeneration in physiology and pathology: the immune signature driving therapeutic plasticity of neural stem cells. *Physiol Rev* 2011;91:1281–304.
- Draijer S, Chaves I, Hoekman MFM. The circadian clock in adult neural stem cell maintenance. *Prog Neurobiol* 2018;173:41–53.
- Ponti G, Obernier K, Guinto C, Jose L, Bonfanti L, Alvarez-Buylla A. Cell cycle and lineage progression of neural progenitors in the ventricular-subventricular zones of adult mice. *Proc Natl Acad Sci U S A* 2013;110:E1045–54.
- Li X, Yang L, Chen LL. The biogenesis, functions, and challenges of circular RNAs. *Mol Cell* 2018;71:428–42.
- Vicens Q, Westhof E. Biogenesis of circular RNAs. *Cell* 2014;159:13–4.
- Jeck WR, Sorrentino JA, Wang K, et al. Circular RNAs are abundant, conserved, and associated with ALU repeats. *RNA* 2013;19:141–57.
- Memczak S, Jens M, Elefsinioti A, et al. Circular RNAs are a large class of animal RNAs with regulatory potency. *Nature* 2013;495:333–8.
- Han B, Zhang Y, Zhang Y, et al. Novel insight into circular RNA HECTD1 in astrocyte activation via autophagy by targeting MIR142-TIPARP: implications for cerebral ischemic stroke. *Autophagy* 2018;14:1164–84.
- Yang L, Han B, Zhang Y, et al. Engagement of circular RNA HECW2 in the nonautophagic role of ATG5 implicated in the endothelial-mesenchymal transition. *Autophagy* 2018;14:404–18.
- Huang R, Zhang Y, Han B, et al. Circular RNA HIPK2 regulates astrocyte activation via cooperation of autophagy and ER stress by targeting MIR124-2HG. *Autophagy* 2017;13:1722–41.
- Du WW, Yang W, Chen Y, et al. Foxo3 circular RNA promotes cardiac senescence by modulating multiple factors associated with stress and senescence responses. *Eur Heart J* 2017;38:1402–12.
- Wang K, Long B, Liu F, et al. A circular RNA protects the heart from pathological hypertrophy and heart failure by targeting miR-223. *Eur Heart J* 2016;37:2602–11.
- Boeckel JN, Jae N, Heumuller AW, et al. Identification and characterization of hypoxia-regulated endothelial circular RNA. *Circ Res* 2015;117:884–90.
- Lui JH, Hansen DV, Kriegstein AR. Development and evolution of the human neocortex. *Cell* 2011;146:18–36.
- Ihrie RA, Alvarez-Buylla A. Lake-front property: a unique germinal niche by the lateral ventricles of the adult brain. *Neuron* 2011;70:674–86.
- Kriegstein A, Alvarez-Buylla A. The glial nature of embryonic and adult neural stem cells. *Annu Rev Neurosci* 2009;32:149–84.
- Ramos AD, Andersen RE, Liu SJ, et al. The long noncoding RNA PNKY regulates neuronal differentiation of embryonic and postnatal neural stem cells. *Cell Stem Cell* 2015;16:439–47.
- Cao Z, Xiao Q, Dai X, et al. circHIPK2-mediated sigma-1R promotes endoplasmic reticulum stress in human pulmonary fibroblasts exposed to silica. *Cell Death Dis* 2017;8:3212.
- Wu F, Han B, Wu S, et al. Circular RNA TLK1 aggravates neuronal injury and neurological deficits after ischemic stroke via miR-335-3p/TIPARP. *J Neurosci* 2019.

- [30] Khelif Y, Toutain J, Quittet MS, et al. A heparan sulfate-based matrix therapy reduces brain damage and enhances functional recovery following stroke. *Theranostics* 2018;8:5814–27.
- [31] Luo CX, Lin YH, Qian XD, et al. Interaction of nNOS with PSD-95 negatively controls regenerative repair after stroke. *J Neurosci* 2014;34:13535–48.
- [32] Fan J, Chen M, Wang X, et al. Targeting SMOX is neuroprotective and ameliorates brain inflammation in cerebral ischemia/reperfusion rats. *Toxicol Sci* 2019;168:381–93.
- [33] Chen Z, Wang H, Zhong J, et al. Significant changes in circular rna in the mouse cerebral cortex around an injury site after traumatic brain injury. *Exp Neurol* 2019;313:37–48.
- [34] Bai Y, Zhang Y, Han B, et al. Circular RNA DLGAP4 ameliorates ischemic stroke outcomes by targeting miR-143 to regulate endothelial-mesenchymal transition associated with blood-brain barrier integrity. *J Neurosci* 2018;38:32–50.
- [35] Song X, Zhang N, Han P, et al. Circular RNA profile in gliomas revealed by identification tool Uroborus. *Nucleic Acids Res* 2016;44:e87.
- [36] Mehta SL, Pandi G, Vemuganti R. Circular RNA expression profiles alter significantly in mouse brain after transient focal ischemia. *Stroke* 2017;48:2541–8.
- [37] Kumar L, Shamsuzzama, Haque R, Baghel T, Nazir A. Circular RNAs: the emerging class of non-coding RNAs and their potential role in human neurodegenerative diseases. *Mol Neurobiol* 2017;54:7224–34.
- [38] van Rossum D, Verheijen BM, Pasterkamp RJ. Circular RNAs: novel regulators of neuronal development. *Front Mol Neurosci* 2016;9:74.
- [39] Fang J, Zhang T, Liu Y, et al. PAX6 downregulates miR-124 expression to promote cell migration during embryonic stem cell differentiation. *Stem Cells Dev* 2014;23:2297–310.
- [40] Cheng LC, Pastrana E, Tavazoie M, Doetsch F. miR-124 regulates adult neurogenesis in the subventricular zone stem cell niche. *Nat Neurosci* 2009;12:399–408.
- [41] Doeppner TR, Doehring M, Bretschneider E, et al. MicroRNA-124 protects against focal cerebral ischemia via mechanisms involving USP14-dependent rest degradation. *Acta Neuropathol* 2013;126:251–65.
- [42] Imitola J, Raddassi K, Park KI, et al. Directed migration of neural stem cells to sites of CNS injury by the stromal cell-derived factor 1alpha/CXC chemokine receptor 4 pathway. *Proc Natl Acad Sci USA* 2004;101:18117–22.
- [43] Yan YP, Sailor KA, Lang BT, Park SW, Vemuganti R, Dempsey RJ. Monocyte chemoattractant protein-1 plays a critical role in neuroblast migration after focal cerebral ischemia. *J Cereb Blood Flow Metab* 2007;27:1213–24.
- [44] Darsalia V, Allison SJ, Cusulin C, et al. Cell number and timing of transplantation determine survival of human neural stem cell grafts in stroke-damaged rat brain. *J Cereb Blood Flow Metab* 2011;31:235–42.
- [45] Drury-Stewart D, Song M, Mohamad O, et al. Highly efficient differentiation of neural precursors from human embryonic stem cells and benefits of transplantation after ischemic stroke in mice. *Stem Cell Res Ther* 2013;4:93.
- [46] Mohamad O, Drury-Stewart D, Song M, et al. Vector-free and transgene-free human iPS cells differentiate into functional neurons and enhance functional recovery after ischemic stroke in mice. *PLoS ONE* 2013;8:e64160.
- [47] Zhao J, Moore AN, Redell JB, Dash PK. Enhancing expression of NRF2-driven genes protects the blood brain barrier after brain injury. *J Neurosci* 2007;27:10240–8.
- [48] El-Husseini AE, Schnell E, Chetkovich DM, Nicoll RA, Brecht DS. PSD-95 involvement in maturation of excitatory synapses. *Science* 2000;290:1364–8.
- [49] Ostroff LE, Fiala JC, Allwardt B, Harris KM. Polyribosomes redistribute from dendritic shafts into spines with enlarged synapses during LTP in developing rat hippocampal slices. *Neuron* 2002;35:535–45.
- [50] Briz V, Restivo L, Pasciuto E, et al. The non-coding RNA BC1 regulates experience-dependent structural plasticity and learning. *Nat Commun* 2017;8:293.
- [51] Nie J, Yang X. Modulation of synaptic plasticity by exercise training as a basis for ischemic stroke rehabilitation. *Cell Mol Neurobiol* 2017;37:5–16.
- [52] Ward NS, Brown MM, Thompson AJ, Frackowiak RS. Neural correlates of outcome after stroke: a cross-sectional fMRI study. *Brain* 2003;126:1430–48.
- [53] Liu Z, Chopp M. Astrocytes, therapeutic targets for neuroprotection and neurorestoration in ischemic stroke. *Prog Neurobiol* 2016;144:103–20.
- [54] Cervelli M, Amendola R, Polticelli F, Mariottini P. Spermine oxidase: ten years after. *Amino Acids* 2012;42:441–50.
- [55] Tomitori H, Usui T, Saeki N, et al. Polyamine oxidase and acrolein as novel biochemical markers for diagnosis of cerebral stroke. *Stroke* 2005;36:2609–13.
- [56] Murray-Stewart T, Wang Y, Goodwin A, Hacker A, Meeker A, Casero Jr. RA. Nuclear localization of human spermine oxidase isoforms - possible implications in drug response and disease etiology. *FEBS J* 2008;275:2795–806.
- [57] Cervelli M, Bellini A, Bianchi M, et al. Mouse spermine oxidase gene splice variants. Nuclear subcellular localization of a novel active isoform. *Eur J Biochem* 2004;271:760–70.
- [58] Murray-Stewart T, Sierra JC, Piazuelo MB, et al. Epigenetic silencing of miR-124 prevents spermine oxidase regulation: implications for helicobacter pylori-induced gastric cancer. *Oncogene* 2016;35:5480–8.